J. Anat. (2008) **212**, pp636–644 doi: 10.1111/j.1469-7580.2008.00881.x

Three-dimensional description and mathematical characterization of the parasellar internal carotid artery in human infants

Stefan Meng,[1,2] Luciano da F. Costa,[3] Stefan H. Geyer,[1] Matheus P. Viana,[3] Christian Reiter,[4] Gerd B. Müller[5] and Wolfgang J. Weninger[1]

[1]*IMG, Center for Anatomy and Cell Biology, Medical University of Vienna, Austria*
[2]*Department of Radiology, Kaiser-Franz-Joseph-Spital, Vienna, Austria*
[3]*Instituto de Física de São Carlos, Universidade de São Paulo, São Carlos, Brazil*
[4]*Department of Forensic Medicine, Medical University of Vienna, Austria*
[5]*Department of Theoretical Biology, University of Vienna, Austria*

Abstract

Inside the 'cavernous sinus' or 'parasellar region' the human internal carotid artery takes the shape of a siphon that is twisted and torqued in three dimensions and surrounded by a network of veins. The parasellar section of the internal carotid artery is of broad biological and medical interest, as its peculiar shape is associated with temperature regulation in the brain and correlated with the occurrence of vascular pathologies. The present study aims to provide anatomical descriptions and objective mathematical characterizations of the shape of the parasellar section of the internal carotid artery in human infants and its modifications during ontogeny. Three-dimensional (3D) computer models of the parasellar section of the internal carotid artery of infants were generated with a state-of-the-art 3D reconstruction method and analysed using both traditional morphometric methods and novel mathematical algorithms. We show that four constant, demarcated bends can be described along the infant parasellar section of the internal carotid artery, and we provide measurements of their angles. We further provide calculations of the curvature and torsion energy, and the total complexity of the 3D skeleton of the parasellar section of the internal carotid artery, and compare the complexity of this in infants and adults. Finally, we examine the relationship between shape parameters of the parasellar section of the internal carotid artery in infants, and the occurrence of intima cushions, and evaluate the reliability of subjective angle measurements for characterizing the complexity of the parasellar section of the internal carotid artery in infants. The results can serve as objective reference data for comparative studies and for medical imaging diagnostics. They also form the basis for a new hypothesis that explains the mechanisms responsible for the ontogenetic transformation in the shape of the parasellar section of the internal carotid artery.

Key words carotid siphon; cavernous sinus; cushion; intimal hyperplasia; vascular remodelling.

Introduction

The human internal carotid artery (ICA) arises from the common carotid artery. It ascends through the parapharyngeal space and enters the skull via the carotid canal. Inside the skull the ICA passes through the so-called cavernous sinus, a network of intracranial veins, before it enters the subarachnoidal space medial to the anterior clinoid process. In the subarachnoidal space it runs occipitally and terminates by branching into the anterior and the middle cerebral arteries. These arteries provide the blood supply to the frontal and parietal parts of the brain. Along its complicated course, which involves several sharp bends, the section of the ICA that runs inside the cavernous sinus is of particular interest. It is hypothesized that the intimate proximity of the double-bent artery to the venous plexus of the sinus cavernous region, which is partly fed by extracranial vessels, is involved in temperature regulation of the rostral parts of the tel- and diencephalon (Brengelmann, 1993; du Boulay et al. 1998; Zhu, 2000). Besides other important structures these regions of the brain include temperature-sensitive nuclei such as the preoptic area, which is responsible for body temperature regulation and

Correspondence
S. Meng, IMG, Center for Anatomy and Cell Biology, Medical University of Vienna, Waehringer Str. 13, A-1090 Vienna, Austria.
E: Stefan.meng@meduniwien.ac.at

Accepted for publication *11 January 2008*

seems to be associated with lifespan (Conti et al. 2006; Saper, 2006). In other mammals, such as artiodactyls, which have a carotid rete or 'rete mirabilis' instead of a single parasellar ICA, the role of temperature exchange is even more accentuated (Jessen, 2001; Fukuta et al. 2007). The reduction of the snout during hominid evolution and the increase of temperature regulation via the skin may have diminished the role of the arterio-venous temperature exchange inside the skull, but the strongly bent shape of the parasellar ICA inside the cavernous sinus may represent a phylogenetic reminiscence of its earlier function.

As the term 'cavernous sinus' is still the subject of debate (Krivosic, 1987; Taptas, 1987; Bonneville et al. 1989; Parkinson, 1995; Weninger et al. 1997; Kehrli et al. 1998; Weninger & Müller, 1999; Weninger & Pramhas, 2000), we prefer to refer to the 'parasellar region', and we term the cavernous sinus segments of the ICA the 'parasellar ICA' (pICA). According to this definition, the pICA starts at the internal ostium of the carotid canal and ends medial to the anterior clinoid process when it penetrates the dura mater and adjacent arachnoidea mater (Fig. 1). Three segments are traditionally distinguished along the pICA (Fischer, 1938): the ascending C5 segment, medial to the trigeminal ganglion, the sagittal C4 segment medial to the abducent nerve, and the curved, again ascending C3 segment that lies first below and later medial to the anterior clinoid process (Fig. 1). In a lateral view the S-shaped configuration of these segments resembles a siphon, hence the traditional term 'carotid siphon', with its posterior knee between segments C5 and C4 and the anterior knee formed by segment C3 (Fischer, 1938; Moniz, 1940). The anterior knee continues into segment C2, which is defined as the proximal part of the ICA inside the subarachnoidal space.

The parasellar segments of the human pICA are well known for the frequent occurrence of vascular pathologies, such as atherosclerotic lesions, aneurysms and extensive intima cushions (Dörfler, 1935; Samuel, 1956; Cole & Davies, 1963; Fisher et al. 1965; Di Chiro & Libow, 1971; Meyer & Lind, 1972; Craig et al. 1982; Marzewski et al. 1982; Borozan et al. 1984; Sakata et al. 1985; Caplan et al. 1986; Wechsler et al. 1986; Raju & Fredericks, 1987; Stary et al. 1992; Kappelle et al. 1999). Intima cushions have been tentatively implicated in sudden infant death syndrome (SIDS) (Weninger et al. 1999). As the pICA undergoes significant changes of shape during postnatal development, there is reason to assume that the remodelling of the vessel walls provides a source for pathological deviations. Such causal connections between changes of shape and the occurrence of pathology are difficult to assert in the absence of quantitative data that define the complex modifications of the shape of the pICA during its development from infant to adult. In this study we introduce a new methodology for the characterization of blood vessel shape and provide comparative shape values for the infant and adult pICA.

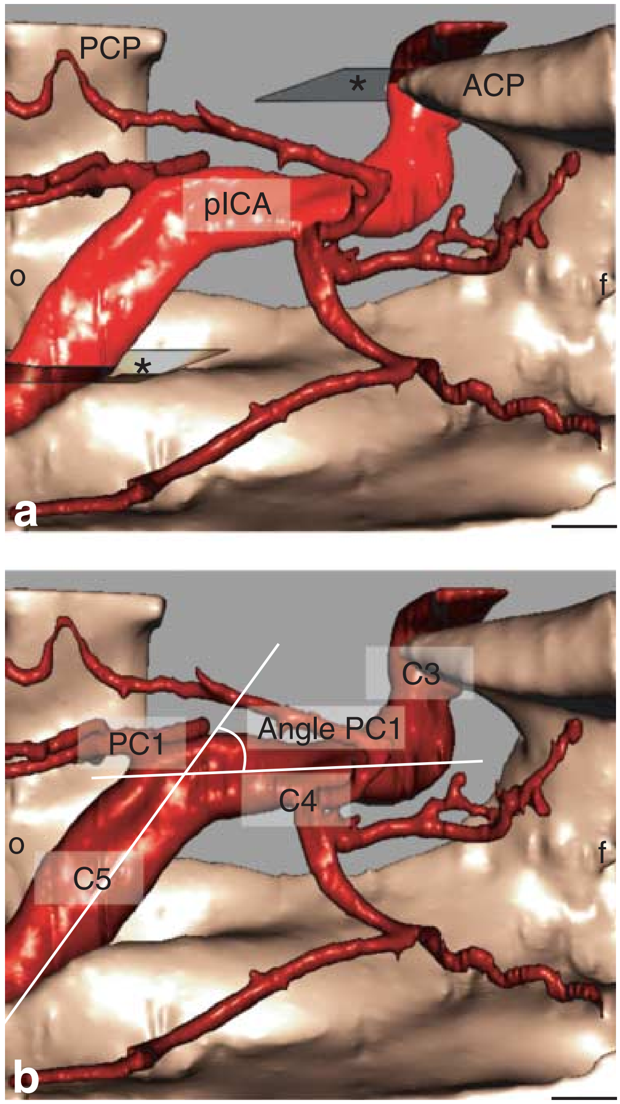

Fig. 1 Three-dimensional computer models of the infant parasellar internal carotid artery (pICA) and its branches *in situ*. Lateral views. (a) Definition of the pICA. Note the virtual cutting planes (asterisks). (b) Segments of the pICA. White lines show how we defined the angle (Angle PC1) of the bend PC1 between Fischer segment C5 (C5) and Fischer segment C4 (C4). f, frontal; o, occipital; PCP, posterior clinoid process; ACP, anterior clinoid process; C3, Fischer segment C3. Scale bar, 1 mm.

Despite long-standing knowledge of its general form, the exact morphology and functionality of the adult human pICA is still poorly understood. Even more scant and contradictory is the information available on the infant pICA, with the exception that its course through the parasellar region is much straighter than in the adult (Schiefer & Vetter, 1957; Jovanovic, 1971; Knosp et al. 1987a; Weninger & Müller, 1999). This lack of information is due to scarce infant material and insufficient quantitative methods. However, knowledge of the shape of the infant pICA is the key to understanding the complex shape of the adult pICA as well as its remodelling, functionality and pathologies.

In adults, several attempts were made to provide objective shape definitions by measuring the angles of the knees of the carotid siphon (Michailow, 1964; Chrzanowski, 1971). These measurements are usually based on lateral (two-dimensional, 2D) projections. However, considering the 3D shape of the pICA, a 2D characterization is a simplification that seriously limits explanatory power. In reality, the adult pICA is bent and twisted in all three dimensions, similar to that of an irregularly shaped screw (Dei Poli & Zucha, 1940). In infants, no serious attempts were undertaken to provide definitions or quantifications of the pICA shape. In this study we aim to provide precise 3D definitions of the shape of the infant pICA by using virtual goniometry and 3D mathematical tools applied to 3D computer models. We further will compare the mathematically calculated complexity of infant and adult pICAs in order to derive an estimate of the changes of shape. Finally, we will examine the frequency of occurrence and the location of intima cushions in infant pICAs in relation to the vessel complexity.

Material and methods

Parasellar regions (PSRs) of 27 human infants (four left, 23 right) were collected during a forensic study and were stored in 3.7% neutral buffered formaldehyde. The infants (nine female, 18 male) were aged between 5 h and 11 months. Mean age was 4.2 months. Twelve infants had died from accidents and 15 were diagnosed with SIDS.

The pICAs were fixed *in situ* and then dissected out of the PSR. Using the EPI-3D method (Weninger et al. 1998), 3D computer models of the vessel lumen, the vessel wall, and of the intima cushions of the pICAs were reconstructed ($6 \times 6 \times 12$ μm and $10 \times 10 \times 12$ μm voxel size). They were visualized and analysed virtually using the software packages Velocity^2 (Minnesota Datametrics) and Amira 4.0 (Mercury Computer Systems), running on a PC. The position and the angles of the curves along the infant pICAs were defined and measured using 2D screenshots of the 3D models after rotating them into the plane formed by each curve (i.e. these are not simple lateral projections of the vessel shape). This procedure closely resembles the method that is usually employed by morphologists for measuring angles of anatomical structures. Measurements were performed using the virtual goniometer tool of the ImageJ software (http://rsb.info.nih.gov/ij). Figure 1 shows how the angles were defined and measured taking the posterior knee of the carotid siphon (PC1) as an example. Subjective interpretation of the blood vessel shape was the basis for the definition of both the angle and the plane in which it was measured.

As objective measures for pICA shape complexity, we provide measurements of the curvature and torsion energy of its 3D skeleton. The pICAs were computationally skeletonized, using an adaptation of the methodology described by Verroust & Lazarus (2000). We considered the skeleton of each pICA as a 3D parametric curve, subsequently fitted by a polynomial of degree 9 (obtained by generalized mean squares fitting). Next, we used differential geometry (Do Carmo, 1976) to estimate the curvature (κ) and torsion (τ) of the curves. We used the Fourier transform to convolve the curve with a Gaussian kernel function with standard deviation σ so as to smooth the original discrete curves, as required in order to eliminate the quantization noise while retaining the main geometrical aspects of the arteries. We selected $\sigma = 10$, which best suited the above request. It is important to observe that this smoothing reduces the amplitude of the signal. To solve this problem, we multiply the coordinates of the smoothed curve by the factor $P_\sigma = L/L_\sigma$, i.e. the ratio between the perimeter of the original curve and the perimeter of the smoothed curve (Sapiro & Tannenbaum, 1995; Cesar & Costa, 1997).

The measures used for characterizing artery geometry are the energies of curvature (E_κ) and torsion (E_τ). Their mathematical definitions are:

$$E_\kappa = L^2 \frac{1}{N} \sum_{i=1}^{N} \kappa_i^2$$

$$E_\tau = L^2 \frac{1}{N} \sum_{i=1}^{N} \tau_i^2$$

where L denotes the length of the pICA. The factor L^2 ensures the energy measures above are scale-invariant, in the sense that a circle will always have the same energy ($E_\kappa^{circle} = 4\pi^2$), independently of its radius. In other words, the energies will be invariant to the scaling of the curves, allowing us to compare pICAs with different lengths (e.g. for adults and infants). The initial and final 10% of the N points along the curves were not considered in the above energies to avoid the discontinuity at the two extremities of the curves. It is important to observe that the energy results are dimensionless, because curvature and torsion have units corresponding to the inverse of the length. We also provide data on total complexity, which we defined as the sum of curvature and torsion.

We also used the 3D skeletons for calculating the angles of the infant pICA. The straightest regions of the skeletons were manually delimited. Next, we applied the principal component analysis methodology to these straightest regions in order that they fit straight lines (corresponding to the main axes). The angles between these lines were then estimated and considered as measures.

For statistics we employed the Wilcoxon rank-sum test and Student's *t*-test, and the Pearson's product moment and Spearman's rank correlation coefficient. All statistical analyses were performed using the SAS software package (SAS Institute Inc.).

Results

We present anatomical characterizations of the infant pICA, calculations of its shape complexity (including comparisons between the infant and adult pICA), and correlations between the infant pICA shape complexity and the occurrence of intima cushions.

Anatomical characterization of the infant pICA

Adult pICAs show two major curves, one between Fischer segments C5 and C4 and a second within Fischer segment C3. No other constant bends can be discerned. The infant pICA, by comparison, takes a relatively straight course and our analysis of the 3D computer models reveals up to five well-demarcated bends. Four of these are present in more than 50% of the specimens. We number the bends from proximal to distal as parasellar curve 1 (PC1), through to

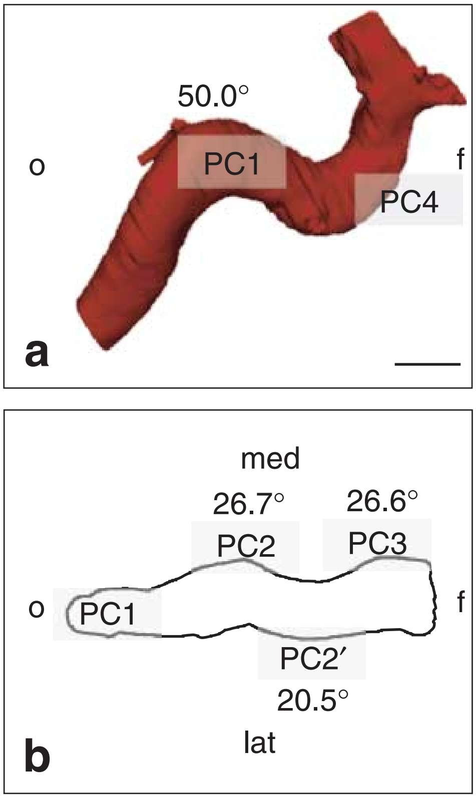

Fig. 2 Bends of the infant pICA. (a) Three-dimensional model viewed laterally. (b) Outline sketch of a 3D model viewed from the top. Note that the curves PC2, PC2′ and PC3 can only be discerned in a top view. Mean dimensions are given for PC1–PC3. f, frontal; o, occipital; med, medial; lat, lateral. Scale bar, 1 mm.

parasellar curve 4 (PC4). PC1 is located at the transition of Fischer segment C5 to C4, PC2 within Fischer segment C4, and PC3 at the proximal part of Fischer segment C3. PC4 corresponds to the proximal part of the anterior knee of the carotid siphon – the curve formed by Fischer segment C3. Of the specimens, 48% show an additional bend in the C4 segment distal to PC2. If present, this bend is named PC2′ (Fig. 2). In the following, we present information about the angles of each bend, first as measured with the aid of a virtual goniometer, and second as calculated from the 3D skeleton of the pICA.

PC1 is present in 100% of the specimens. It is orientated in a sagittal plane, with its apogee directed dorsally. Goniometric angle measurements ranged from 17 to 108.5°, with a mean of 50° and a median of 45° (SD 25.3°). Mathematical calculations of the same angle ranged from 18.4 to 100°, with a mean of 52.8° and a median of 48.4° (SD 24.7°).

PC2 is present in 100%. It is orientated in a transverse plane, with its apogee directed laterally in 85% and medially in 15%. Goniometric angle measurements range from 5 to 75°, with a mean of 26.7° and a median of 24° (SD 16.4°). Mathematical calculations of the same angle ranged from 8.3 to 88.6°, with a mean of 36° and a median of 31° (SD 22°).

PC2′ occurs in 48% of the specimens. Like PC2 it is orientated in a transverse plane, but the apogee of PC2′ is always directed to the opposite direction of that of PC2. In 69% this direction is medial, in 31% lateral. Goniometric angle measurements range from 6 to 38.5°, with a mean of 20.5° and a median of 17° (SD 10°). Mathematical calculations of the same angle ranged from 6.4 to 65.1°, with a mean of 34.1° and a median of 34.5° (SD 16.3°).

PC3 is present in 74% of the specimens. It is located at the transition zone of Fischer segments C3 and C4 and orientated in a transverse plane. Its apogee points medially in 58% and laterally in 42%. Goniometric angle measurements range from 3 to 64°, with a mean of 26.6° and a median of 24° (SD 14.6°). Mathematical calculations of the same angle ranged from 10.1 to 85.2°, with a mean of 37.7° and a median of 35.8° (SD 22.6°).

PC4 is observed in 100% of the specimens. It is the proximal part of the curve usually described as the anterior knee of the carotid siphon. This curve continues along the subarachnoidal C2 segment of the ICA, which is not a part of the excised pICA section. This prevents angle measurements.

For all measured angles the paired Student's *t*-test revealed significant differences between the goniometric angle measures and the mathematical calculations of the angles. Pearson's product moment test revealed strong and significant correlations.

Mathematical complexity of the infant pICA

Beside goniometric measurements, a mathematical analysis of curvature and torsion energy and total complexity was performed in order to obtain an objective mathematical characterization of the infant pICA. The curvature energy of the infant pICA ranged from 0.63 to 7.60 with a mean of 2.95 (SD 2.15). Torsion energy ranged from 0.01 to 4.70 with a mean of 1.04 (SD 1.15). Total complexity, as defined by the sum of curvature and torsion energy, ranged from 0.76 to 11.66 with a mean of 3.99 (SD 2.93). Curvature and torsion energy showed a significant correlation ($r = 0.475$, $P = 0.0123$).

We evaluated the significance and objectivity of goniometric measures for characterizing the complexity of the infant pICA. First, we summed the angles PC1–PC3. Values ranged from 30 to 237.5°, with a mean of 106.4°. Statistical comparisons revealed significant correlations between curvature energy and the sum of the goniometrically measured angles ($r = 0.543$, $P = 0.0034$) (Fig. 3a), torsion energy and the sum of the goniometrically measured angles ($r = 0.574$, $P = 0.0017$), and total complexity and the sum of the goniometrically measured angles ($r = 0.643$, $P = 0.0003$). Secondly, we compared only angle PC1 with the mathematical indicators of complexity. Statistics revealed a strong correlation between the dimension of PC1 and curvature energy ($r = 0.737$, $P < 0.0001$) (Fig. 3b) and a positive correlation between the dimension of PC1 and

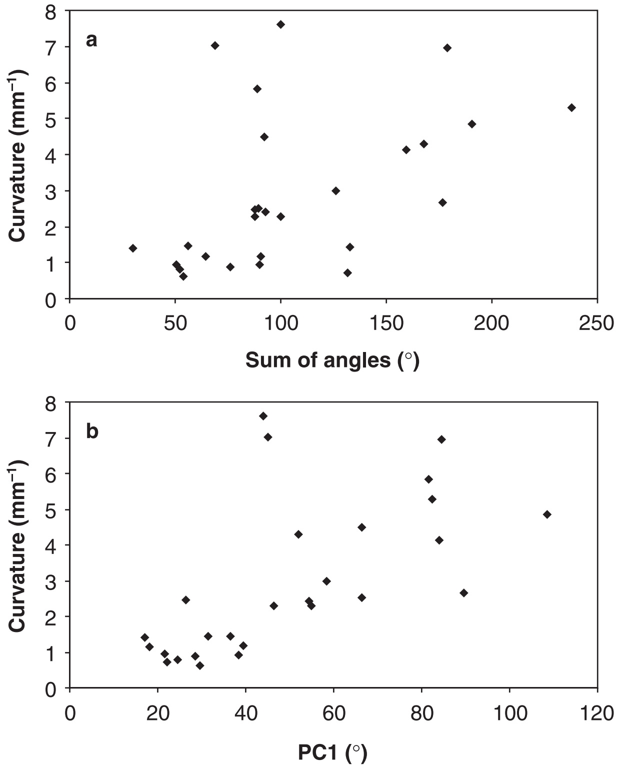

Fig. 3 Correlation between subjective goniometric measurements and curvature energy. (a) Comparison between curvature energy and sum of the angles PC1–PC3. (b) Comparison between curvature and PC1.

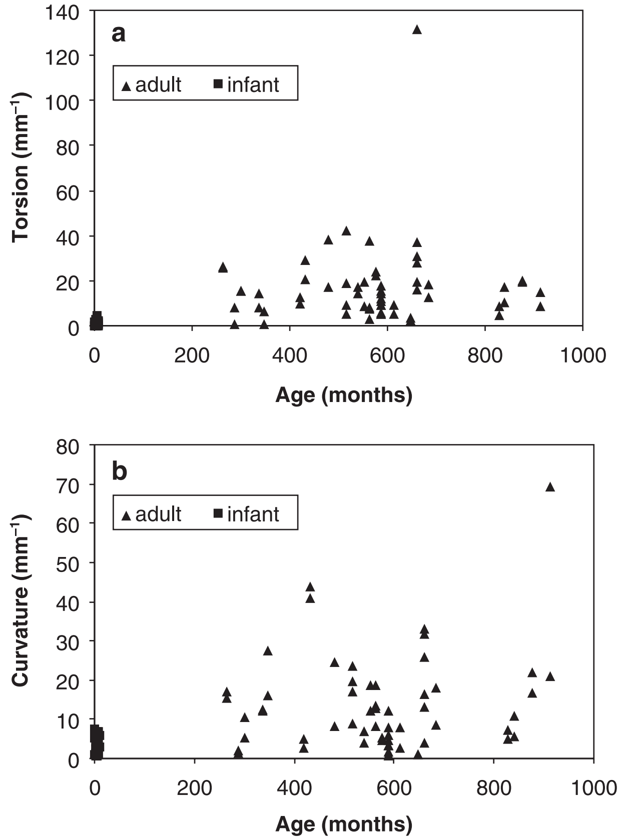

Fig. 4 Comparisons of the mathematical indicators of complexity between infant and adult pICAs. (a) Torsion energy. (b) Curvature energy.

total energy ($r = 0.702$, $P < 0.0001$). A weak, non-significant correlation was seen between PC1 and torsion energy ($r = 0.314$, $P = 0.1113$).

In order to elucidate the characteristics of ontogenetic transformations occurring during childhood and adolescence, we compared curvature and torsion energies and total complexity of infant and adult pICAs. The adult pICA shows a mean curvature energy of 12.99, a mean torsion energy of 16.71 and a mean total complexity of 29.70 (sample size 60 pICAs; S. Meng et al. unpublished data). The mean curvature energy ($P < 0.0001$), the mean torsion energy ($P < 0.0001$) and the mean total complexity ($P < 0.0001$), defined as the sum of curvature and torsion energy, was significantly higher in adults than in infants (Fig. 4). The pICA curvature for 24 (40%) adults was smaller than 7.6, the pICA torsion for 6 (10%) adults was smaller than 4.7, and the pICA total complexity of 10 (17%) adults was smaller than 11.66. In these cases the dimensions of the objective shape parameters were similar to that of infants (Fig. 4).

Intima cushions of the infant pICA

Intima cushions occur at constant locations in each segment of the pICA (Fig. 5a). Their precise location, extension, histological structure and degree of lumen occlusion have been described previously (Weninger et al. 1999). Here we investigated the topology and occurrence of intima cushions and their relationship to pICA complexity in the present sample. C5 cushions were found in 67% of our specimens, C4 cushions in 81% and C3 cushions in 56%. A weak, non-significant correlation was found for curvature energy and the number of intima cushions ($r = 0.3148$, $P = 0.1097$) as well as for the total complexity and the number of intima cushions ($r = 0.33983$, $P = 0.0829$) (Fig. 5). No correlation was found for the torsion energy and the number of intima cushions ($r = 0.18421$, $P = 0.3577$). Wilcoxon rank sum tests revealed no significant differences of curvature energy between pICAs with and without a C3 cushion ($P = 0.3229$), C4 cushion ($P = 0.4472$) or C5 cushion ($P = 0.1936$); no significant differences in torsion energy between pICAs with and without a C3 cushion ($P = 0.7551$), C4 cushion ($P = 0.2078$) or C5 cushion ($P = 0.4632$); and no significant differences in total complexity between pICAs with and without a C3 cushion ($P = 0.3473$), C4 cushion ($P = 0.2845$) or C5 cushion ($P = 0.1311$). Statistical comparison of SIDS cases with the victims of accidents revealed no significant differences in the shapes of the pICA or the presence of intima cushions.

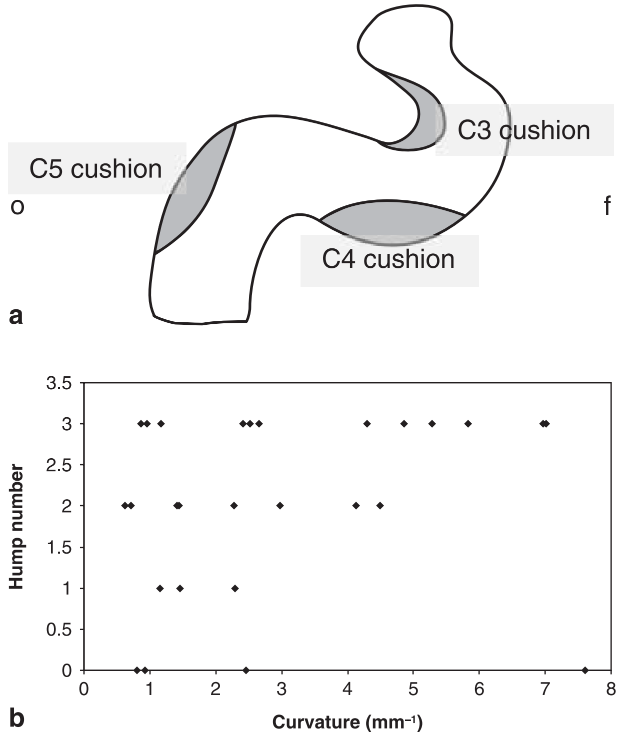

Fig. 5 Intima cushions of the infant pICA. (a) Location. (b) Correlation between number of intima cushions and curvature energy. o, occipital; f, frontal.

Discussion

The topology and course of the pICA is of clinical and scientific significance. Therefore, a number of attempts were undertaken to provide geometric and numeric descriptions of the shape of the adult pICA (Fischer, 1938; Dei Poli & Zucha, 1940; Moniz, 1940; Curry & Culbreth, 1951; Platzer, 1957; Schiefer & Vetter, 1957; Kozlowski, 1963; Udvarhelyi et al. 1963; Michailow, 1964; Bergland et al. 1968; Chrzanowski, 1971; Jovanovic, 1971; Hasso et al. 1975; Knosp et al. 1988). In contrast, information on the shape of the infant pICA is scant (Schiefer & Vetter, 1957; Jovanovic, 1971; Weninger & Müller, 1999). Numerical definitions are only available for the bend between Fischer segment C5 and C4 and are of limited significance. However, detailed characterizations of the infant pICA shape and complexity are of importance for two reasons. First, forerunners of vascular pathologies occur already in infants and are considered to be linked to the complexity of the 3D shape of the pICA (Meyer & Lind, 1972; Weninger et al. 1999). Second, no sufficient explanations exist for the peculiar shape of the adult pICA and the ontogenetic factors responsible for this shape. The present study provides, for the first time, detailed descriptions and careful measurements of the infant pICA using modern 3D reconstruction techniques. It also provides objective mathematical characterizations of the pICA, and compares the complexity of the infant pICA shape with that of adults. These comparisons can serve as a starting point for elucidating the ontogenetic mechanisms and the pathogenic effects of pICA shape complexity.

For comparisons with existing data, we analysed the 3D computer models with classical anatomical methods and detected four constant curves along the infant pICA (PC1–PC4). The bend we termed PC1 corresponds to the posterior knee of the carotid siphon and is located at the transition of Fischer segment C5 to C4. There are two possible ways to characterize this bend, first by measuring the angle formed by virtual lines through the C5 and C4 segment, and second by measuring the angle between the C4 segment and the straight continuation of the C5 segment. We chose the latter, because this angle represents the degree of deviation from the originally straight course of the fetal pICA. In adult anatomical specimens, PC1 measures between 15 and 120° (Michailow, 1964), which corresponds to 60–165° in our measurement protocol. In infants we measured angles between 17 and 108.5° (mean 49.43°). Thus, although the infant PC1 shows the same broad individual variability, in general it is much straighter than the adult pICA. The last bend of the infant pICA (PC4) is part of the anterior knee of the so-called carotid siphon. Its angle could not be measured as the bend continues in the C2 segment.

Of peculiar interest are the bends between PC1 and PC4. The second bend of the infant pICA (PC2) in the C4 segment, the third bend (PC3) in the proximal C3 segment and the inconstant PC2′ are blunt. However, these bends are well demarcated and are regular features of the infant pICA. No such angles can be discerned in the adult pICA, which is formed like a helix or corkscrew, nor in the fetal pICA, which takes a very straight course, only bent around the transition zone from Fischer segment C3 to C2 (Knosp et al. 1987b). PC2, PC2′ and PC3 thus are unique features of the infant pICA.

Goniometric angle measurements were made from images showing 2D projections of the pICA. For each bend, the best fitting projection image is subjectively defined by the researcher. Although this procedure represents the traditional way to define angles, such measurements neglect the 3D components of a curve. To overcome this problem and to provide truly objective angle measures for each bend, we mathematically skeletonized the blood vessels. The 3D skeleton of a blood vessel represents a 3D curve. We identified the straight sections in this curve and calculated the angles with the aid of principal components analysis.

We also used the 3D skeletons for mathematical analysis of the complexity of the shape of the entire pICA. The relevant geometrical features and the complexity of the 3D skeleton of the pICA can be precisely expressed as its curvature (κ) and the torsion (τ), which are both invariant to the translation and rotation of the curve. In addition to their intrinsic interpretation, curvature and torsion provide a complete representation of the curve, in the sense that the latter can be recovered from the values obtained for curvature and torsion. Preliminary investigations of the geometry of arteries have been reported (Ding & Friedman, 2000; Zhu & Friedman, 2003; Medina et al. 2004). The Fourier transform has been used in order to estimate curvature and torsion (Costa & Cesar, 2001; Costa, 2002). Ding & Friedman (2000) proposed the use of piecewise interpolation by low degree polynomials for estimating the curvature and torsion of 3D arteries. A comparison between these two approaches, reported in Medina et al. (2004), indicated better estimation of curvature by using the Fourier approach. The more unstable torsion can be calculated more properly by the piecewise approach. We consider the skeleton of each pICA as a 3D parametric curve, subsequently fitted by a polynomial of degree 9 (obtained by generalized mean squares fitting) and used differential geometry (Do Carmo, 1976) to estimate its curvature (κ) and torsion (τ).

Using the mathematical methods, we found that infant pICAs show remarkable individual variations in torsion and curvature energy. However, curvature and torsion energy of the pICAs correlate positively. While torsion is a measure for the intrinsic twisting along the longitudinal axis of the artery, curvature defines a structure's complexity based on its curves. Consequently, curvature energy does show a strong correlation with the goniometrically measured sum of the pICA angles and an even stronger correlation with the dimension of PC1. In contrast, torsion energy is only correlated with the sum of the angles PC1–PC3 and does not significantly correlate with the dimension of PC1. This implies that the sum of the measurable angles of the infant pICA does provide a fair estimation of the objective complexity of the blood vessel. However, the identification and measuring of pICA angles is time consuming and laborious and requires the use of advanced 3D reconstruction methods. The angle of PC1, in contrast, can be easily and quickly measured in the traditional, subjectively biased way. However, although we show that PC1 is an excellent representative for the amount of curvature energy, it does not permit a sound estimation of torsion energy and thus is a poor indicator for the real complexity of the infant pICA.

We provide comparisons between the mathematical complexity (curvature and torsion) of the infant and the adult pICA. Data for the adult pICA await publication (S. Meng et al. in preparation). The data are based on an analysis of 3D models of 60 pICAs of 30 randomly selected patients (22–77 years) without pathologies or of near the parasellar region. The 3D models were reconstructed from contrast media enhanced computed tomography scans. Statistics show that the mean curvature and torsion energy and the total complexity are much lower in the infant pICA than in the adult pICA. While the mean curvature energy of adult pICAs is approximately four times higher than that of infant pICAs, the mean torsion energy of adult pICAs is approximately 16 times higher than that of infant pICAs. Therefore, we concluded that extensive vascular remodelling occurs during childhood and adolescence and leads to an increase of the objectively measurable blood vessel complexity. This increase, however, is mainly due to an increase in torsion energy.

Cushion-like protrusions that narrow the lumen of the vessel at characteristic positions are a regular finding in the pICA of human infants (Fig. 5). However, while bent infant pICAs with an acute angle PC1 show such cushions, straight running blood vessels with a very blunt angle PC1 lack them (Weninger et al. 1999). Thus, we expected to identify cushions more frequently in pICAs of higher complexity. Surprisingly the present study, which is based on 27 infant specimens, reveals that neither the number nor the presence of intima cushions due to intimal hyperplasia correlates with the mathematically calculated measures of pICA complexity. No differences in curvature, torsion or total complexity can be seen between pICAs with and without a C3, C4 and C5 cushion. As we assume that blood flow characteristics vary with blood vessel complexity, these findings suggest that intimal hyperplasia of the infant pICA is not, or at least not entirely, caused by haemodynamic forces. Intima hyperplasia is considered as a forerunner of atherosclerosis (Stary et al. 1992). Therefore, our data suggest that individuals with a complex pICA and individuals with a less complex pICA have the same risk of atherosclerosis of the pICA and associated disorders.

Along its course from neck to brain, the ICA adheres via its adventitia to the walls of the carotid canal and via ligaments to the anterior clinoid process (Knosp et al. 1988). Therefore, both the proximal end of the pICA, which is attached to the internal opening of the carotid canal, and its distal end, which is attached to the anterior clinoid process, are fixed points with respect to the skull base. A long stretch of the pICA is in contact only with its surrounding venous plexus. Based on our findings we suggest a model that could explain the transformations of the pICA from its straight shape in infants to the heavily twisted shape in adults.

We argue that in prenatal life the distance between the internal opening of the carotid canal and the base of the anterior clinoid process and the length of the pICA increase synchronously. Hence, the pICA of the fetus runs straight through the parasellar region (Knosp et al. 1987a). In the perinatal period skull base growth and pICA length growth become slightly asynchronous, with the pICA lengthening faster than the distance between the internal opening of the carotid canal and the basis of the anterior clinoid process. Therefore, the pICA develops its torsion and two pronounced as well as 2–3 blunt, but well-demarcated bends, the apogee of which point in opposite directions. During childhood and adolescence, blood vessel length increases rapidly, while the skull base dimensions increase at a slower rate. This forces the pICA to find its way through the parasellar space by forming a helix – a shape that would automatically result from increasing the length of a proximally and distally fixed tube inside a given volume. Formation of the helix shape results in elimination of the defined blunt bends PC2–PC3. Spatial constraints are just one ontogenetic factor responsible for the pICA shape transformation. Haemodynamic forces may also trigger vascular remodelling and postnatal pICA transformation. We suggest that these haemodynamic forces cause an accentuation of the more acute bends of the infant pICA, which are PC1 and PC4. Therefore, the adult pICA does not simply show a helix shape, as caused by the spatial constraints, but a helix shape with two prominent bends – the anterior and posterior knee of the carotid siphon. We postulate that both haemdoynamic forces and spatial constraints are involved in the formation of the complex shape of the adult pICA.

Acknowledgements

L.dF.C. thanks FAPESP (05/00587-5) and CNPq (308231/03-1) for financial support. M.P.V. thanks FAPESP (07/50882-9).

References

Bergland RM, Ray BS, Torack RM (1968) Anatomical variations in the pituitary gland and adjacent structures in 225 human autopsy cases. *J Neurosurg* **28**, 93–99.

Bonneville JF, Cattin F, Dietemann JL (1989) Hypothalamic–pituitary region: computed tomography imaging. *Baillieres Clin Endocrinol Metab* **3**, 35–71.

Borozan PG, Schuler JJ, LaRosa MP, Ware MS, Flanigan DP (1984) The natural history of isolated carotid siphon stenosis. *J Vasc Surg* **1**, 744–749.

du Boulay GH, Lawton M, Wallis A (1998) The story of the internal carotid artery of mammals: from Galen to sudden infant death syndrome. *Neuroradiology* **40**, 697–703.

Brengelmann GL (1993) Specialized brain cooling in humans? *Faseb J* **7**, 1148–1153.

Caplan LR, Gorelick PB, Hier DB (1986) Race, sex and occlusive cerebrovascular disease: a review. *Stroke* **17**, 648–655.

Cesar RM Jr, Costa L da F (1997) Application and assessment of multiscale bending energy for morphometric characterization of neural cells. *Rev Sci Intrum* **68**, 2177–2186.

Chrzanowski R (1971) The assessment of the intracranial part of the internal carotid artery. *Neuroradiology* **2**, 223–226.

Cole M, Davies H (1963) Carotid siphon calcification. *Br J Radiol* **36**, 289–293.

Conti B, Sanchez-Alavez M, Winsky-Sommerer R, et al. (2006) Transgenic mice with a reduced core body temperature have an increased life span. *Science* **314**, 825–828.

Costa L da F, Cesar RM Jr (2001) *Shape Analysis and Classification: Theory and Practice*. Boca Raton, FL: CRC Press.

Costa L da F (2002) Estimating derivatives and curvature of open curves. *Pattern Recognition* **35**, 2445–2451.

Craig DR, Meguro K, Watridge C, Robertson JT, Barnett HJ, Fox AJ (1982) Intracranial internal carotid artery stenosis. *Stroke* **13**, 825–828.

Curry RW, Culbreth GC (1951) The normal cerebral angiogram. *AJR Am J Roentgenol* **65**, 345–373.

Dei Poli G, Zucha J (1940) Beiträge zur Kenntnis der Anomalien und der Arteria carotis interna. *Zentralblatt Neurochirurgie* **5/6**, 209–238.

Di Chiro G, Libow LS (1971) Carotid siphon calcification and cerebral blood flow in the healthy aged male. *Radiology* **99**, 103–107.

Ding Z, Friedman MH (2000) Dynamics of human coronary arterial motion and its potential role in coronary atherogenesis. *J Biomech Eng* **122**, 488–492.

Do Carmo M (1976) *Differential Geometry of Curves and Surfaces*. Englewood Cliffs, NJ: Prentice-Hall.

Dörfler J (1935) Ein Beitrag zur Frage der Lokalisation der Arteriosklerose der Gehirngefäße mit besonderer Berücksichtigung der arteria carotis interna. *Arch Psychiatr* **103**, 180–190.

Fischer E (1938) Die Lageabweichung der vorderen Hirnarterie im Gefäßbild. *Zentralblatt Neurochirurgie* **5**, 300–317.

Fisher CM, Gore I, Okabe N, White PD (1965) Calcification of the carotid siphon. *Circulation* **32**, 538–548.

Fukuta K, Kudo H, Sasaki M, Kimura J, bin Ismail D, Endo H (2007) Absence of carotid rete mirabile in small tropical ruminants: implications for the evolution of the arterial system in artiodactyls. *J Anat* **210**, 112–116.

Hasso AN, Bentson JR, Wilson GH, Vignaud J (1975) Neuroradiology of the sphenoidal region. *Radiology* **114**, 619–627.

Jessen C (2001) Selective brain cooling in mammals and birds. *Jpn J Physiol* **51**, 291–301.

Jovanovic S (1971) [Variations and development of the internal carotid artery curves in the cavernous sinus]. *Glas Srp Akad Nauka [Med]* **23**, 163–173.

Kappelle LJ, Eliasziw M, Fox AJ, Sharpe BL, Barnett HJ (1999) Importance of intracranial atherosclerotic disease in patients with symptomatic stenosis of the internal carotid artery. The North American Symptomatic Carotid Endarterectomy Trail. *Stroke* **30**, 282–286.

Kehrli P, Ali M, Reis M Jr, et al. (1998) Anatomy and embryology of the lateral sellar compartment (cavernous sinus) medial wall. *Neurol Res* **20**, 585–592.

Knosp E, Müller G, Perneczky A (1987a) Anatomical remarks on the fetal cavernous sinus and on the veins of the missle cranial fossa. In *The Cavernous Sinus: A Multidisciplinary Approach to Vascular and Tumorous Lesions* (ed. Dolenc VV), pp. 104–116. Vienna: Springer Verlag.

Knosp E, Müller G, Perneczky A (1987b) The blood supply of the cranial nerves in the lateral wall of the cavernous sinus. In *The Cavernous Sinus: A Multidisciplinary Approach to Vascular and Tumorous Lesions* (ed. Dolenc VV), pp. 67–80. Vienna: Springer Verlag.

Knosp E, Müller G, Perneczky A (1988) The paraclinoid carotid artery: anatomical aspects of a microneurosurgical approach. *Neurosurgery* **22**, 896–901.

Kozlowski P (1963) Relation of the internal carotid siphon to the carotid sulcus. *Acta Radiol* **1**, 328–331.

Krivosic I (1987) Histoarchitecture of the cavernous sinus. In *The Cavernous Sinus* (ed. Dolenc VV), pp. 117–129. Berlin: Springer.

Marzewski DJ, Furlan AJ, St Louis P, Little JR, Modic MT, Williams G (1982) Intracranial internal carotid artery stenosis: longterm prognosis. *Stroke* **13**, 821–824.

Medina R, Wahle A, Om E, Sonka M (2004) Curvature and torsion estimation for coronary-artery motion analysis. *Proc SPIE* **5369**, 504–515.

Meyer WW, Lind J (1972) Calcifications of the carotid siphon – a common finding in infancy and childhood. *Arch Dis Child* **47**, 355–363.

Michailow SS (1964) Makro-und mikroskopische Untersuchungen des Baues des Sinus cavernosus. *Anat Anz* **115**, 233–255.

Moniz E (1940) Die cerebrale Arteriographie und Phlebographie. In *Handbuch der Neurologie* (eds Bumke O, Foerster O), pp. 62–66. Berlin: Julius Springer.

Parkinson D (1995) Lateral sellar compartment: history and anatomy. *J Craniofac Surg* **6**, 55–68.

Platzer W (1957) Die Variabilität der Arteria carotis interna im Sinus cavernosus in Beziehung zur Variabilität der Schädelbasis. *Gegenbaurs Morphologisches Jahrbuch* **98**, 227–243.

Raju S, Fredericks RK (1987) Carotid siphon stenosis. *J Cardiovasc Surg (Torino)* **28**, 671–677.

Sakata N, Joshita T, Ooneda G (1985) Topographical study on arteriosclerotic lesions at the bifurcations of human cerebral arteries. *Heart Vessels* **1**, 70–73.

Samuel KC (1956) Atherosclerosis and occlusion of the internal carotid artery. *J Path Bact* **71**, 391–401.

Saper CB (2006) Biomedicine. Life, the universe, and body temperature. *Science* **314**, 773–774.

Sapiro G, Tannenbaum A (1995) Area and length preserving geometric invariant scale-spaces. *IEEE Trans PAMI* **17**, 67–72.

Schiefer W, Vetter K (1957) Das zerebrale Angiogramm in den verschiedenen Altersstufen. *Zentralblatt Neurochirurgie* **17**, 218–231.

Stary HC, Blankenhorn DH, Chandler AB, et al. (1992) A definition of the intima of human arteries and of its atherosclerosis-prone regions. A report from the Committee on Vascular Lesions of the Council on Arteriosclerosis, American Heart Association. *Arterioscler Thromb* **12**, 120–134.

Taptas JN (1987) Must we still call cavernous sinus the parasellar vascular and nervous crossroads? The necessity of a definite topographical description of the region. In *The Cavernous Sinus* (ed. Dolenc VV), pp. 30–40. Berlin: Springer.

Udvarhelyi GB, Langfitt TW, Cox A (1963) Neuroradiologic diagnostic procedures in suprasellar space-occupying lesions with special reference to angiographic measurements. *Acta Radiol* **1**, 485–508.

Verroust A, Lazarus F (2000) Extracting skeletal curves from 3D scattered data. *The Visual Computer* **16**, 15–25.

Wechsler LR, Kistler JP, Davis KR, Kaminski MJ (1986) The prognosis of carotid siphon stenosis. *Stroke* **17**, 714–718.

Weninger WJ, Streicher J, Müller GB (1997) Anatomical compartments of the parasellar region: adipose tissue bodies represent intracranial continuations of extracranial spaces. *J Anat* **191**, 269–275.

Weninger WJ, Meng S, Streicher J, Müller GB (1998) A new episcopic method for rapid 3-D reconstruction: applications in anatomy and embryology. *Anat Embryol (Berl)* **197**, 341–348.

Weninger WJ, Müller GB (1999) The parasellar region of human infants: cavernous sinus topography and surgical approaches. *J Neurosurg* **90**, 484–490.

Weninger WJ, Müller GB, Reiter C, Meng S, Rabl SU (1999) Intimal hyperplasia of the infant parasellar carotid artery: a potential developmental factor in atherosclerosis and SIDS. *Circ Res* **85**, 970–975.

Weninger WJ, Pramhas D (2000) Compartments of the adult parasellar region. *J Anat* **197**, 681–686.

Zhu H, Friedman MH (2003) Relationship between the dynamic geometry and wall thickness of a human coronary artery. *Arterioscler Thromb Vasc Biol* **23**, 2260–2265.

Zhu L (2000) Theoretical evaluation of contributions of heat conduction and countercurrent heat exchange in selective brain cooling in humans. *Ann Biomed Eng* **28**, 269–277.